Reply to "Comments on 'Potential Vorticity Mixing and Rapid Intensification in the Numerically Simulated Supertyphoon Haiyan (2013)'"

SATOKI TSUJINO[a] AND HUNG-CHI KUO[b]

[a] *Faculty of Environmental Earth Science, Hokkaido University, Sapporo, Hokkaido, Japan*
[b] *Department of Atmospheric Sciences, National Taiwan University, Taipei, Taiwan*

(Manuscript received 11 March 2021, in final form 29 June 2021)

KEYWORDS: Hurricanes/typhoons; Tropical cyclones; Potential vorticity

Tsujino and Kuo (2020, hereafter TK20) is the sequel paper of Kuo et al. (2019, hereafter K19) to study the inner-core dynamics of Supertyphoon Haiyan (2013) undergoing rapid intensification (RI) with a 2-km resolution cloud-resolving model simulation from the nonhydrostatic Cloud-Resolving Storm Simulator (CReSS; Tsuboki and Sakakibara 2002). K19 uses dynamic energy efficiency (DEF) to aid the RI diagnosis, in which the efficacy of convective heating at any point in generating kinetic energy can be calculated. The results highlight the nonlinear feedback process in which deep convection becomes collocated with the large DEF area near the eyewall and the large unbalanced radial inflow in the boundary layer to generate the deep convective potential vorticity (PV) tower in the eyewall. TK20 employed a piecewise PV inversion (PPVI) to interpret the model results with balanced dynamics. At the low level in the simulated storm, the PV field reveals an elliptical and polygonal-shaped eyewall during RI onset. The PV budget analysis in TK20 confirms the importance of PV mixing at this stage, i.e., the asymmetric transport of diabatically generated PV to the storm center from the eyewall and the ejection of PV filaments outside the eyewall. The PPVI indicates that PV mixing accounts for about 50% of the central pressure fall during RI onset. The decrease of central pressure enhances the boundary layer (BL) inflow. The BL inflow leads to contraction of the radius of the maximum tangential wind (RMW) and the formation of a symmetric convective PV tower inside the RMW. The results suggest that the pressure change associated with PV mixing, the increase of the symmetric unbalanced BL radial inflow, and the development of a symmetric convective PV tower are the essential collaborating dynamics for RI. The PV mixing and diagnosis in TK20 is in general agreement with Hendricks and Schubert (2010). TK20 also indicates the importance of the model resolution in the simulation of the eyewall convective PV tower. The peak PV value in convective PV tower is 60 PVU (200 PVU; 1 PVU = 10^{-6} K kg^{-1} m^2 s^{-1}) at 2-km (500-m) resolution. TK20 focused on the contribution of the low-level PV mixing to the surface pressure decrease. The contribution of the upper warm core 14–16 km above the surface pressure decrease is somewhat ignored.

Shi and Chen (2021, hereafter SC21) have two major comments on TK20. The first comment is on the method of TK20 used to separate the individual contributions of the upper- and lower-level eye warming to the low-level vortex central pressure decrease. Specifically, SC21 argued that the air density decrease at the warm core at 14–16-km heights (Fig. 1 in SC21) will contribute to the pressure decrease "deep level below" as illustrated in Fig. 2 of SC21. In particular, the maximum perturbation pressure due to the 14–16-km warm anomaly is near the surface (Fig. 2c in SC21). In addition, SC21 argues that the contribution of the perturbation pressure is more significant from the 14–16-km warm anomaly than that in the 4–6-km layer (Figs. 2c and 2d in SC21). The calculation of the pressure anomaly in SC21 is based on the hydrostatic equation integrated downward from the model top with virtue temperature variable as in Zhang and Chen (2012). The second comment is that the balanced geopotential height perturbations (i.e., the pressure deficits) inverted from the piecewise PV may involve significant contributions from the processes irrelevant to the PV mixing. Specifically, SC21 speculated that in TK20 the PV anomalies in the eyewall may have a larger contribution to the central pressure decrease than those of the same magnitude in the eye region after the PV mixing. SC21 cited the result of Kieu and Zhang (2010, hereafter KZ10) to support their argument.

Our reply to the first comment of SC21 is in three parts. First, the local warm anomaly's contribution to pressure cannot be studied solely with the hydrostatic equation as is in SC21. The hydrostatic balance implicitly assumes that no horizontal variation exists. As a consequence, the entire response to a density perturbation in a column is confined to that column. In reality, elevated temperature perturbation source of finite horizontal extent quickly provokes an acoustic response in the surrounding environment that efficiently spreads the pressure perturbations horizontally. The dynamics are the hydrostatic adjustment and the calculation is the anelastic pressure equation solving. The anelastic pressure calculation is valid in the buoyancy time scale of N^{-1} (Ogura and Phillips 1962). For a high-altitude source, the response is large immediately above and below the source but decreases in magnitude very quickly away from the source location as expected from the very nature of the elliptical equation. The surface pressure perturbation

Corresponding author: Hung-Chi Kuo, kuo@as.ntu.edu.tw

DOI: 10.1175/JAS-D-21-0070.1

response to the high-altitude source is nearly undetectable. In the time scale $N^{-1} < t < f^{-1}$, a time scale between the buoyancy time scale and Coriolis time scale, the PV thinking is not a useful tool for dynamic analysis. The anelastic pressure argument is true with or without the Coriolis effect. In time scale $t > f^{-1}$, the anelastic pressure equation is still valid, but the factor such as geostrophic adjustment may become more important.

The second part of the response is to a longer time scale when the Coriolis effect is important. In such a time scale, gravity waves spread the pressure (mass) perturbation while the Coriolis factor may alter the spread somewhat and turns some signal into the wind information. In a vortex environment, the vortex rotation or the vortex inertial stability poses an additional dynamic barrier for the horizontal spread of the pressure perturbations. Likewise, the vortex static stability controls the vertical penetration. The equilibrium pressure or geopotential height response should be studied with both gradient wind balance and hydrostatic balance equations together. The dynamics are the hydrostatic–geostrophic adjustment and the calculation is the PV invertibility. Figure 1 shows the geopotential height anomalies from the PPVI with a constant PV anomaly confined at different altitudes in the pseudoheight (pressure) vertical coordinate. The vortex basic state and PV anomaly are from TK20. Figure 1a shows the height anomaly is limited to the upper atmosphere for the PV anomaly confined above a height of 11 km (i.e., the upper warm layer in TK20). The height deficit pattern in Fig. 1a is an elliptical shape with a larger horizontal elongation. The shape is an indication of the Rossby length and the Rossby height of the vortex environment at the upper atmosphere (cf. Schubert and McNoldy 2010). The warm anomaly in the upper region of a tropical cyclone is in an environment of weak inertial stability and strong static stability. The mass or the pressure, according to the geostrophic adjustment, is to spread preferentially to the horizontal direction with a very limited vertical penetration. Figure 1a is in general agreement with Fig. 3d in KZ10, which also clearly showed the pressure anomaly is confined in the upper level.[1] Figures 1b and 1c, the height deficit values with PV anomalies in the middle and lower atmosphere, indicate much more significant height deficit responses and deeper vertical penetrations as can be expected with the larger Rossby height and smaller Rossby length with the lower-level of the storm. Figures 1b and 1c, in that with much larger peak deficit values and deeper vertical penetrations, appear to be in general agreement with the invertibility study such as that in KZ10 (e.g., their Fig. 3f).

The third part of the response is to the discrepancy in the vertical potential temperature profile between the invertibility calculation and that the hydrostatic reasoning of SC21, which is also related to SC21's second comment (i.e., a larger contribution of the PV anomalies in the eyewall to the central pressure decrease). The invertibility calculations indicate that potential temperature anomalies exhibited positive (negative) signs above (below) the PV anomaly peak height (not shown). For the PV anomalies in the eyewall, our calculation and that of Fig. 3e of KZ10 clearly indicated the existence of cold anomalies below the peak height of the PV anomalies. The low-level cold anomalies can contribute to the weakening of the geopotential height deficit (and increase in surface pressure) at the level because potential temperature anomaly (θ') inverted from a PV anomaly is proportional to vertical gradient of the geopotential height anomaly (ϕ') [i.e., $\theta' = (\theta_0/g)\partial\phi'/\partial\hat{z}$, where $\theta_0 = 300$ K, g is gravitational acceleration, and $\hat{z}$ is pseudoheight]. The maximum pressure deficit can be induced by the warm core above the peak height of the positive PV anomaly, and the pressure deficit below the peak height is weakened downward associated with the cold core below the peak height of the PV anomaly. Such negative potential temperature anomalies do not show up in SC21's hydrostatic calculation in the case of the upper warm core, in which the deficit increase cumulatively all the way down to the surface.[2] Without these negative potential temperature anomalies, SC21's calculation might overestimate the contribution of the upper warm core to the surface pressure fall. At least, the discrepancy in the vertical potential temperature profiles indicates that the contribution of the upper warm core to the surface pressure fall based on the hydrostatic calculation in SC21 does not correspond to the surface pressure fall associated with the eyewall PV anomalies.

The method in TK20 assumes that the pressure perturbation in the warm-core layer is directly due to warm-core-induced density anomalies in the layer, and the contribution of the warm-core layer to the surface pressure fall is estimated by the accumulation of the air density including density anomalies in the layer. Namely, only the direct pressure contribution of the upper-level warm anomaly is discussed in Fig. 1 of TK20. While the hydrostatic calculation of TK20 is in general agreement with PPVI, we concede that it is better to use the hydrostatic–geostrophic adjustment to highlight the importance of the low-level PV dynamics. Based on the above discussion, we think it is a questionable argument of SC21 that the warm anomaly at the 14–16-km layer contributes significantly to the "deep level below" and resulted in a very significant pressure deficit in the low level during the RI onset.

Our reply to SC21's speculation that in TK20 the eyewall PV is more important than the eye core PV in contributing to the low-level pressure gradient is as follows. In response to the

[1] The reviewer commented that Fig. 3d in KZ10 indicated a PV anomaly centered at $z = 12.5$ km, with a pressure deficit extending down to $z = 6$–7 km, rather than just being confined in the PV anomaly layer. The authors disagree with the comment because Fig. 3d in KZ10 has a contour interval of 0.05 hPa. The apparent downward extension is a very small pressure deficit. The maximum pressure deficit of Fig. 3d in KZ10 is only 0.4 hPa, and the region of the maximum deficit is confined in the upper layer.

[2] According to SC21's interpretation and Figs. 2a and 2c in SC21, the upper warm core can decrease pressure in the lower troposphere without a temperature change. Thus, the potential temperature must increase in the lower troposphere.

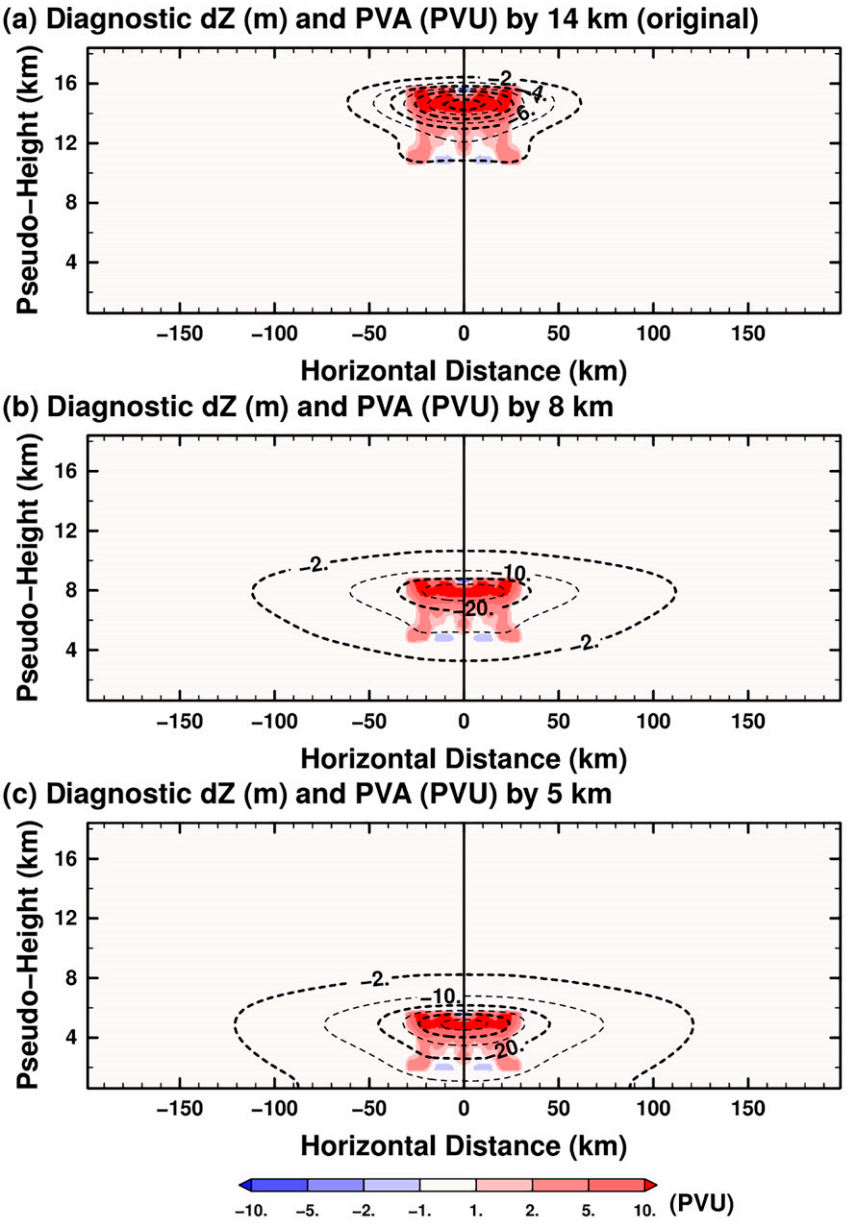

FIG. 1. (a)–(c) Spatial distributions of PV anomalies (colors; PVU) during 0000–0600 UTC 7 Nov 2013 and geopotential height (contours; m) deficits inverted by the PV anomalies. The contours are given at −2 m in (a) and every −10 m in (b) and (c). The PV anomalies in (a) are given in an annular volume with a radius of 20 km in a layer from 11 to 16 km, which is extracted from the actual change in the model simulation shown in Fig. 2e. The PV anomalies in (b) and (c) are given by moving the PV anomalies in (a) to the middle layer (with the peak height of 8 km) and lower layer (with the peak height of 5 km).

question of SC21 that the piecewise PV may involve significant contributions from the processes irrelevant to the PV mixing, Fig. 2 shows decompositions of asymmetric PV advection (i.e., the ASADV term in TK20) in the PV budget results during the RI onset (0000–0600 UTC 7 November 2013) in TK20. The ASADV term is dominated by the horizontal component within a radius of 30 km (Figs. 2a–c). The horizontal component of ASADV within the radius of 30 km is more precisely defined as the PV anomalies associated with the PV mixing (Fig. 2d). Note that the eyewall PV generation is defined by the actual change of PV in a cylindrical area with radii of 30–40 km (Figs. 2e,f), as suggested by SC21. The

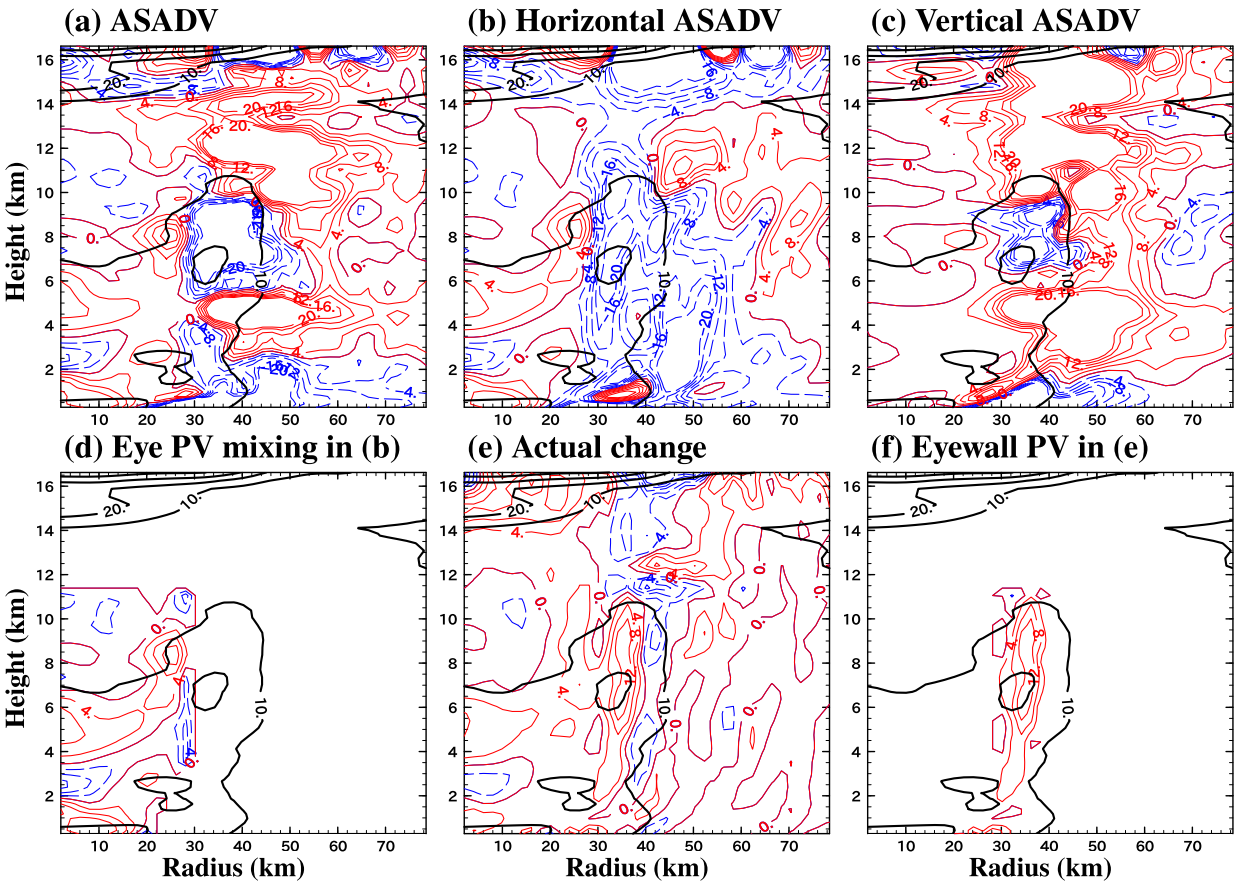

FIG. 2. Radius–height cross sections of (a) total PV advection associated with asymmetric flows (ASADV) (b) the horizontal and (c) the vertical decompositions in the ASADV term, and (e) the actual change of $\overline{P}$ during 0000–0600 UTC 7 Nov 2013 (color contours; PVU for 6 h). (d) The PV anomaly associated with the PV mixing inside the eyewall in (b). (f) The eyewall PV generation, defined as the positive PV tendencies along the eyewall in the actual PV change for 6 h [i.e., (e)]. Black contour denotes $\overline{P}$ (black contours; PVU) averaged over the 6 h. The cross sections in (a) and (e) are identical to Figs. 6e and 6a in TK20, respectively.

budget study in Fig. 2 clearly indicates that the PV mixing is from the eyewall to the eye. Figure 3 provides the height anomaly due to each PV anomaly in the eye core (Fig. 3b) and eyewall (Fig. 3c) from the simulation in TK20 (Fig. 3a). It is clear that PV near the eyewall does not dominate the pressure contribution as speculated by SC21. Our result is somewhat different from that in Fig. 3e of KZ10. There is a significant pressure response to the eyewall PV anomaly in KZ10. Then what is the reason for the difference? Figure 4 is our calculation from the TK20 vortex, which is the same as the vortex used in Fig. 3, with the PV invertibility from a series of idealized eyewall PV anomalies of different horizontal widths. The idealized eyewall PV anomalies (Q_e) are formed by a formulation of $Q_e = A_1 \exp\{-[(z - z_c)/H_e]^2 - [(r - r_c)/R_e]^2\}$ based on Eq. (9a) of KZ10. The parameters for the idealized PV anomalies are $A_1 = 12$ PVU, $H_e = 2$ km, $r_c = 30$ km, and $z_c = 5$ km. The different horizontal widths are specified by the parameter R_e (Fig. 4). The point is that the pressure response (the mass response) depends on the horizontal width of the eyewall PV anomaly according to the geostrophic adjustment theory. An eyewall PV anomaly with a small horizontal scale cannot have a significant pressure signature. In other words, the pressure ingredient of the PV is insignificant when the horizontal width of PV is narrow. Note that SC21's speculation on the importance of eyewall PV anomaly is based on KZ10 in which, for example, eyewall PV anomaly in Fig. 3e (KZ10) has a relatively wide horizontal scale of 30 km and thus a significant pressure response can be expected. TK20 highlights the importance of high resolution to simulate the horizontally sharp feature of convective PV tower. The small horizontal width eyewall PV will not lead to a strong pressure response as shown in Fig. 3c. The PV mixing can be viewed as a dynamic process enlarging the horizontal width of PV in the eye core and make the pressure ingredient of PV important. The sharp convective PV tower and very narrow sharp PV can be further referenced in the modeling study by Hausman et al. (2006) and the observational study of Martinez et al. (2019). Finally, we note that the width and maximum value of the PV generation in the eyewall may increase during the later stages of the RI period (e.g., ST-III and ST-IV in TK20), compared to

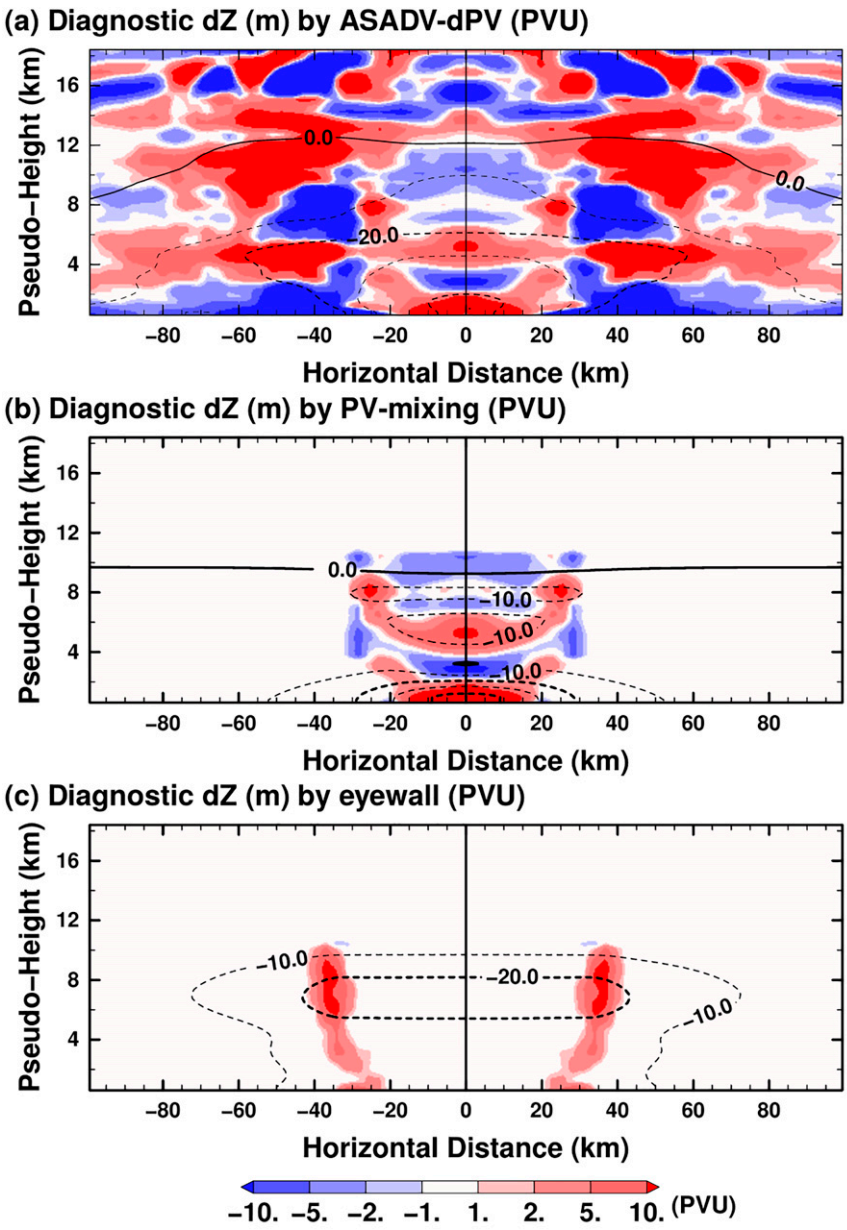

FIG. 3. Spatial distributions of geopotential height (contours; 10 m) deficits and PV anomalies (colors; PVU) during 0000–0600 UTC 7 Nov 2013 corresponding to (a) ASADV in the PV budget by TK20, (b) the PV mixing between the eye and eyewall shown in Fig. 2d, and (c) the PV generation in the eyewall shown in Fig. 2f. (a) As in Fig. 7c in TK20.

those at the early stage of RI. It indicates that, during the later stages of RI when the storm is stronger, the eyewall PV may contribute more to the vortex central pressure decrease.

In summary, SC21 stressed the important contribution of 14–16-km warm anomaly to the surface pressure with hydrostatic calculation. Their calculation is solely based on the hydrostatic balance which may exaggerate the influence of upper-level warm anomaly on the low-level pressure deficit. A more proper discussion in the vortex environment should be based on the hydrostatic–geostrophic adjustment and involved PV invertibility calculation. Warm anomalies at 14–16-km altitude of vortex environment with large Rossby length and small Rossby height, the pressure response is small and is with limited vertical extent. We demonstrate in this reply that the vertical penetration and the magnitude of the height/pressure deficit response depends crucially on the PV anomaly's altitude in the vortex environment. On SC21's speculation that eyewall PV contributes significantly to

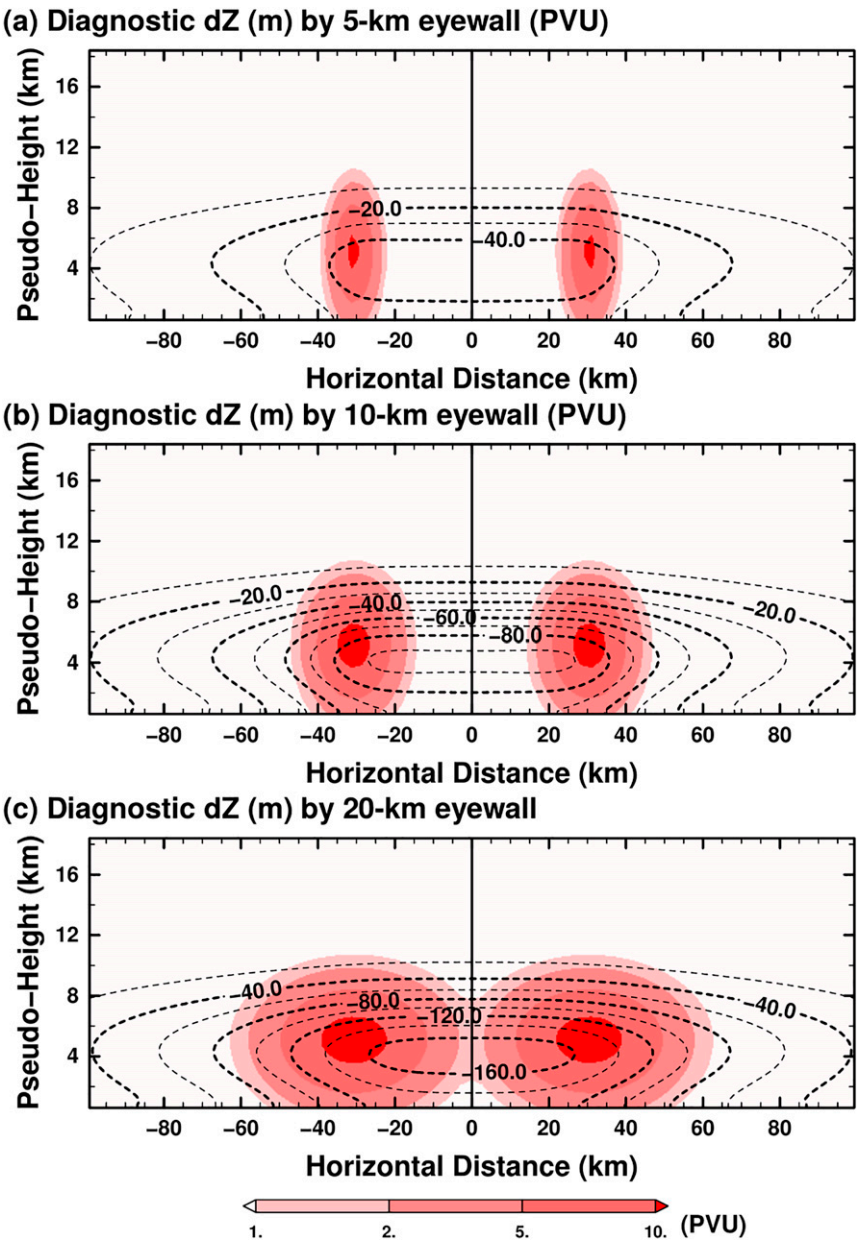

FIG. 4. Spatial distributions of geopotential height deficits (contours; m) for the eyewall PV anomalies (colors; PVU) with different widths (R_e) of (a) 5, (b) 10, and (c) 20 km. The basic vortex is from TK20.

pressure anomaly, our model results indicate otherwise during the onset stage of RI. With a similar background inertial stability factor in mind, the pressure response to the eyewall PV anomaly depends on the horizontal width of the PV anomaly. The sharp feature of eyewall PV may have a weaker pressure ingredient according to the geostrophic adjustment theory. TK20 highlights the pressure gradient due to the PV mixing in driving BL nonlinear inflow and the formation of a very sharp symmetric convective PV tower in the RI. We appreciate the comments of SC21 as the proper partition of pressure and wind ingredient of the eyewall PV anomaly may depend on the model resolution to resolve the sharp eyewall convective PV tower in the RI process.

Acknowledgments. We are grateful to Prof. R. Fovell for the helpful discussion on the acoustic adjustment and shared with us the numerical results of anelastic pressure response to an elevated finite heat source. We thank Prof. D.-L. Zhang and one anonymous reviewer for helpful and thoughtful comments on this reply manuscript. This study was supported by the Ministry of Science and Technology (MOST)

of Taiwan under Grants MOST-109-2111-M-002-008 and MOST-109-2625-M-002-021 and by the Ministry of Education, Culture, Sports, Science and Technology (MEXT) of Japan under JSPS Grant-in-aid JP19H00705. We thank the support of the National Center for Theoretical Sciences, Mathematics Division.

REFERENCES

Hausman, S. A., K. V. Ooyama, and W. H. Schubert, 2006: Potential vorticity structure of simulated hurricanes. *J. Atmos. Sci.*, **63**, 87–108, https://doi.org/10.1175/JAS3601.1.

Hendricks, E. A., and W. H. Schubert, 2010: Adiabatic rearrangement of hollow PV towers. *J. Adv. Model. Earth Syst.*, **2** (4), https://doi.org/10.3894/JAMES.2010.2.8.

Kieu, C. Q., and D.-L. Zhang, 2010: A piecewise potential vorticity inversion algorithm and its application to hurricane inner-core anomalies. *J. Atmos. Sci.*, **67**, 2616–2631, https://doi.org/10.1175/2010JAS3421.1.

Kuo, H.-C., S. Tsujino, C.-C. Huang, C.-C. Wang, and K. Tsuboki, 2019: Diagnosis of the dynamic efficiency of latent heat release and the rapid intensification of Supertyphoon Haiyan (2013). *Mon. Wea. Rev.*, **147**, 1127–1147, https://doi.org/10.1175/MWR-D-18-0149.1.

Martinez, J., M. M. Bell, R. F. Rogers, and J. D. Doyle, 2019: Axisymmetric potential vorticity evolution of Hurricane Patricia (2015). *J. Atmos. Sci.*, **76**, 2043–2063, https://doi.org/10.1175/JAS-D-18-0373.1.

Ogura, Y., and N. A. Phillips, 1962: Scale analysis of deep and shallow convection in the atmosphere. *J. Atmos. Sci.*, **19**, 173–179, https://doi.org/10.1175/1520-0469(1962)019<0173:SAODAS>2.0.CO;2.

Schubert, W. H., and B. D. McNoldy, 2010: Application of the concepts of Rossby length and Rossby depth to tropical cyclone dynamics. *J. Adv. Model. Earth Syst.*, **2** (3), https://doi.org/10.3894/JAMES.2010.2.7.

Shi, D., and G. Chen, 2021: Comments on "Potential vorticity mixing and rapid intensification in the numerically simulated Supertyphoon Haiyan (2013)." *J. Atmos. Sci.*, **78**, 2643–2648, https://doi.org/10.1175/JAS-D-20-0364.1.

Tsuboki, K., and A. Sakakibara, 2002: Large-scale parallel computing of cloud resolving storm simulator. *High Performance Computing*, H. P. Zima et al., Eds., Springer, 243–259.

Tsujino, S., and H.-C. Kuo, 2020: Potential vorticity mixing and rapid intensification in the numerically simulated Supertyphoon Haiyan (2013). *J. Atmos. Sci.*, **77**, 2067–2090, https://doi.org/10.1175/JAS-D-19-0219.1.

Zhang, D.-L., and H. Chen, 2012: Importance of the upper-level warm core in the rapid intensification of a tropical cyclone. *Geophys. Res. Lett.*, **39**, L02806, https://doi.org/10.1029/2011GL050578.